# September Arctic sea-ice minimum predicted by spring melt-pond fraction

**David Schröder\*, Daniel L. Feltham, Daniela Flocco and Michel Tsamados**

The area of Arctic September sea ice has diminished from about 7 million km² in the 1990s to less than 5 million km² in five of the past seven years, with a record minimum of 3.6 million km² in 2012 (ref. 1). The strength of this decrease is greater than expected by the scientific community, the reasons for this are not fully understood, and its simulation is an on-going challenge for existing climate models[2,3]. With growing Arctic marine activity there is an urgent demand for forecasting Arctic summer sea ice[4]. Previous attempts at seasonal forecasts of ice extent were of limited skill[5-9]. However, here we show that the Arctic sea-ice minimum can be accurately forecasted from melt-pond area in spring. We find a strong correlation between the spring pond fraction and September sea-ice extent. This is explained by a positive feedback mechanism: more ponds reduce the albedo; a lower albedo causes more melting; more melting increases pond fraction. Our results help explain the acceleration of Arctic sea-ice decrease during the past decade. The inclusion of our new melt-pond model[10] promises to improve the skill of future forecast and climate models in Arctic regions and beyond.

Ponds form on Arctic sea ice from the accumulation of surface melt during spring and affect the heat and mass balances of the ice cover, mainly by decreasing the value of the mean surface albedo by up to 20% (refs 10,11). Although observations have shown an increase in melt-ponds on Arctic sea[11], little is known about the role of melt-ponds in controlling the sea-ice mass balance and none of the current climate and forecast models use a physically based melt-pond model. We have developed a new melt-pond model suitable for forecasting the evolution of melt-ponds[10] and incorporated this model into the widely applied Los Alamos sea-ice model called CICE (ref. 12). We studied the temporal and spatial evolution of ponds (Figs 1 and 2) from a 35-year-long CICE simulation (1979–2013) for the pan-Arctic region forced with atmospheric NCEP_Reanalysis-2 data[13]. (See Methods for a description of the pond model and the set-up of our simulation.) Our simulations show that melt ponds start to form in May, a maximum extent of 18% is reached in the climatological mean at mid-July, and there are hardly any exposed ponds left by mid-August. The strong inter-annual variability and the positive trend are striking. Whereas in 1996, the year with the highest September ice extent since 1979, the maximum pond fraction reaches only 11%, in 2012, the year with the lowest September ice extent, up to 34% of the sea ice is covered by ponds. Locally the maximum monthly means (of more than 40% in 2012) occur in the border zone between the Arctic Basin and the Laptev Sea, East Siberian Sea and Chuckchi Sea, as well as in Baffin Bay (Fig. 2). The results of our CICE simulation are consistent with *in situ* observations[14,15] and pond statistics for the period 2002–2011 based on MODIS satellite data[16].
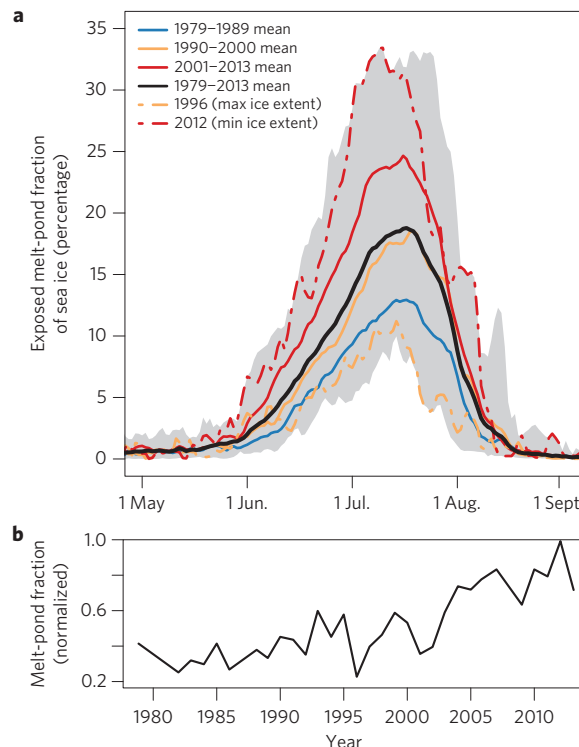
**Figure 1 | Temporal variability of Arctic melt-pond area. a**, Annual cycle of Arctic mean fraction of sea-ice area covered by exposed melt-ponds in our CICE simulation. The grey-shaded area shows the range of pond fraction simulated over the 35-year period. **b**, Time series of normalized pond fraction (mean over the period from 25 June to 25 July).

To quantify the relationship between melt-pond fraction and the sea-ice minimum in the subsequent September, we calculate the correlation between the 35-year time series (1979–2013) of mean Arctic September sea-ice extent (from SSM/I; ref. 1) with the time series of mean Arctic pond area fraction from our CICE simulation. On the basis of the full data sets we calculate weights for each grid point based on the correlation coefficient between the local pond area and the Arctic September ice extent (see Fig. 2 for an example and Methods for details). It is important to state that all time series had been de-trended beforehand. Previous studies[5,9] show a strong correlation between absolute time series of ice and ocean variables with September ice extent, but no skill in predicting de-trended sea-ice extent for lead times of three months and longer. Figure 3 reveals that there is a highly significant correlation (*p*-values < 0.005)

CPOM, Department of Meteorology, University of Reading, PO Box 243, Reading, RG6 6BB, UK. *e-mail: D.Schroeder@reading.ac.uk
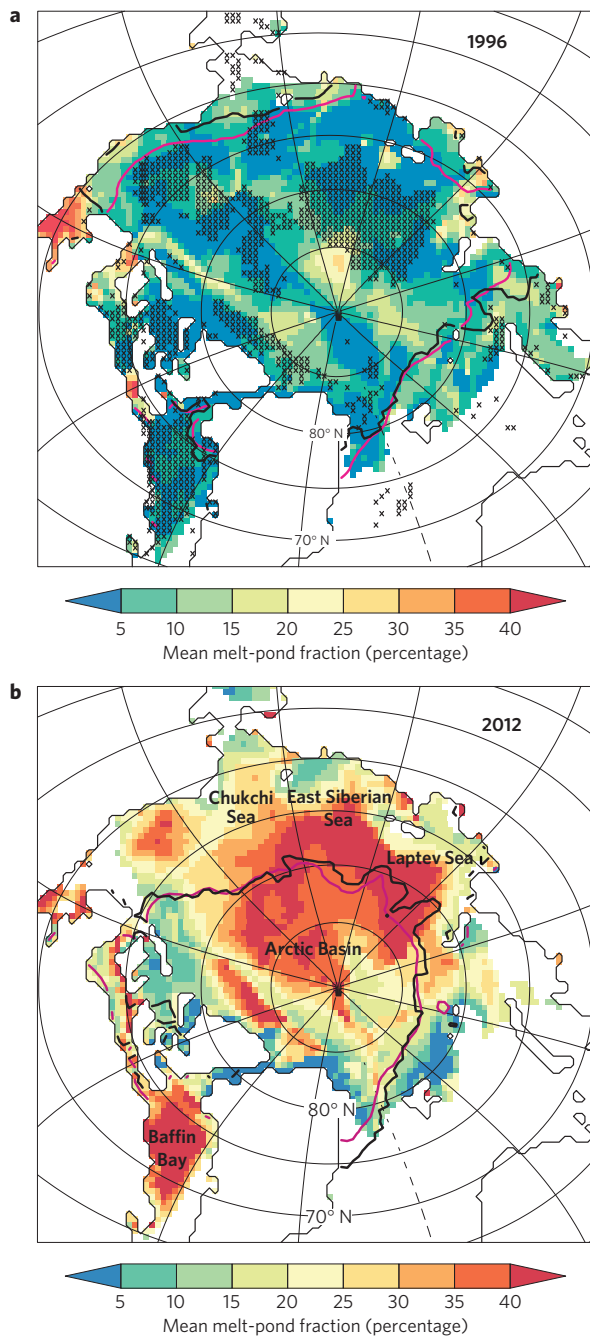
**Figure 2 | Spatial distribution of Arctic melt-pond area.** Mean pond area over the period from 25 June to 25 July for 1996 (**a**) and 2012 (**b**). The purple line is the September ice extent of the same year from our CICE simulation, and the black line is the ice extent from SSM/I. Crosses mark those grid points where mean pond area (1 May to 25 July) is strongly correlated with SSM/I September ice extent (correlation coefficient $R < -0.3$) over the period 1979–2013.

between simulated pond fraction and SSM/I September ice extent. The highest correlation coefficient of $R = -0.80$ occurs for ice extent if the pond area is integrated from 1 to 31 May. Extending the integration time period does not improve the correlation. Although the pond area integrated from 1 to 31 May contains only around 1% of the annually integrated pond area (Fig. 1), the melt-pond fraction in May seems to have the strongest impact on the sea-ice state in the subsequent September. Our results confirm that the early melt season is decisive for the strength of the summer ice retreat[17].
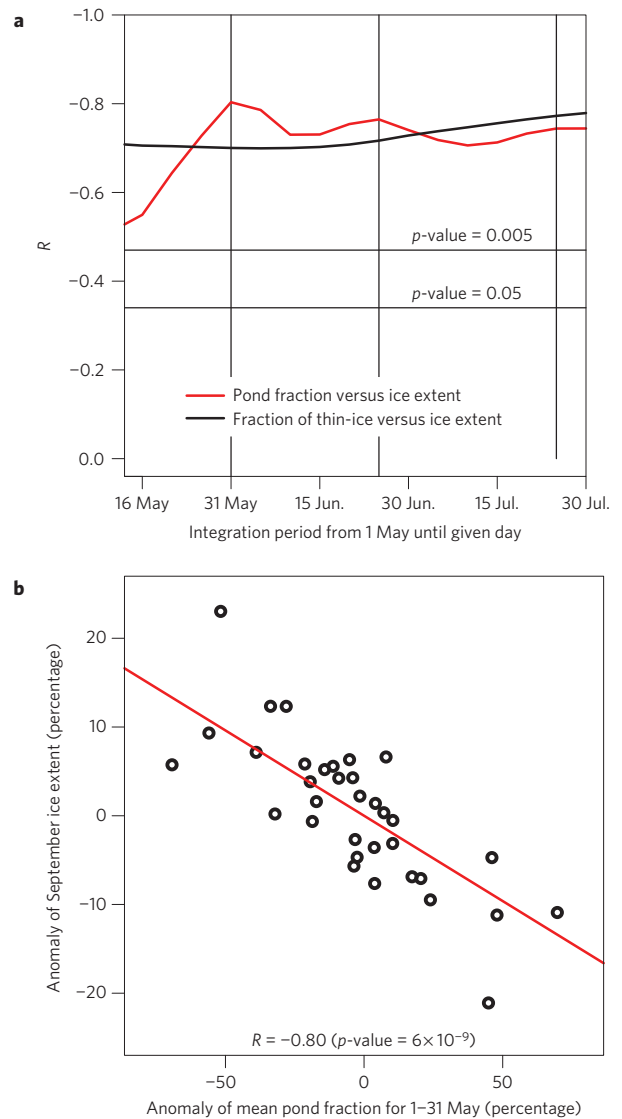


**Figure 3 | Correlation between pond and thin-ice fraction with September sea-ice extent.** The mean Arctic pond and thin-ice fraction are integrated from 1 May until the day given. The Arctic September ice extent is from SSM/I. **a**, Pearson's correlation coefficient $R$ and $p$-values for de-trended time series. The vertical lines indicate the integration periods shown in Fig. 4. **b**, Scatter plot for the May pond fraction and September ice extent. Anomalies are given as a percentage of the mean value. A linear function has been fit to the data (red line).

The September ice extent is known to depend both on the state of the ice in spring (for example, amount of thin ice) and on the atmospheric conditions in the Arctic during summer (for example, wind direction; refs 18,19). To place our results for melt-ponds in context we calculated the correlation between the fraction of thin ice (lowest two ice categories in the model; that is, ice thinner than 1.4 m) with September ice extent using the same integration time periods. The correlation is strongly significant, but the coefficients are lower for thin-ice fraction than for pond area fraction using integration periods up to the end of June (Fig. 3a). Note that there is no significant correlation between the May and June ice area and September ice extent (Supplementary Fig. 1).

Why is there such a strong correlation between pond area fraction in spring and the state of September sea ice? The albedo of ponded sea ice (varying between 0.15 and 0.45) is considerably lower than the albedo of snow-covered or bare ice (generally between 0.50
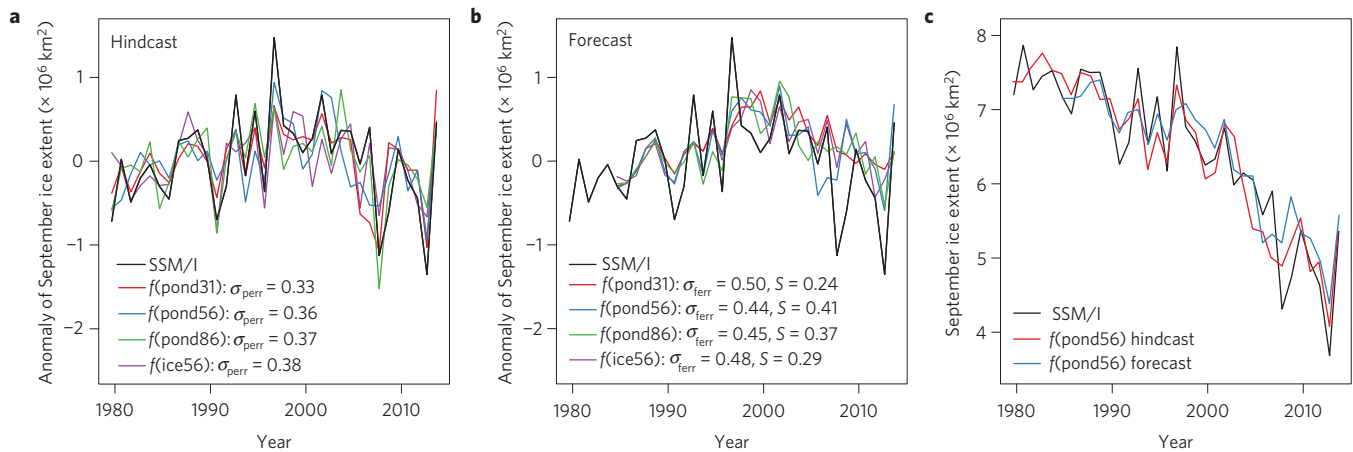
**Figure 4 | Verification of predicted September sea-ice extent.** Predicted ice extent (anomaly from the trend line in **a** and **b** and absolute values in **c**) is verified by use of SSM/I data for the period 1979–2013. Hindcasts (**a**) and forecasts (**b**) are based on three different integration periods for pond fraction: 1 May–31 May (pond31), 1 May–25 June (pond56) and 1 May–25 July (pond86) and one for fraction of thin ice: 1 May–25 June (ice56). $\sigma_{\text{ferr}}$ and $\sigma_{\text{perr}}$ are the prediction and the forecast error in million km$^2$. The given skill values $S$ are with respect to the variance of the de-trended climatology. See Methods for details.

and 0.95; refs 10,17). Ponds cause a strong increase of melting, and that increase in melt water leads to an increase in pond fraction. The degree of increase depends on the ice conditions: the same amount of melt water can cover a larger area over level first-year ice than over rough multi-year ice. This positive feedback mechanism, substantiated with high-resolution process modelling studies[20], gives a physical explanation as to why the amount of ponds, in particular in the early melt season, contributes to the amount of summer ice melt and consequently the amplitude of the minimum ice extent. Furthermore, in our model simulation the location of ponds and pond fraction depend mainly on the location and amount of thin first-year ice and on the heat balance at the air–ice/snow surface. Therefore, pond fraction encompasses important elements of the pre-conditioning of the ice state in late spring with respect to the September ice extent.

To investigate the potential of pond fraction as a predictor for Arctic September sea ice, we first used the whole data period to derive the linear regression between spring pond fraction and September ice extent and applied the regression line to calculate September ice extent from spring pond fraction (hindcast mode). Figure 4a shows that our predicted September ice extent captures the inter-annual variability of the observations well. Our prediction error, $\sigma_{\text{perr}} = 0.33$ million km$^2$, for a prediction based on pond fraction in May is remarkably low. It is fundamentally impossible to determine the September ice extent from the spring pond fraction perfectly, because the impact of the atmospheric and oceanic conditions in July–September are not accounted for refs 8,19. To quantify the dominant impact of the wind forcing (dependence of minimum ice extent on ice dynamics; refs 18,19), for each of the 35 years we performed sensitivity studies starting on 26 June and applied the wind forcing of each year. The resulting variance of September ice extent amounts to 0.15 million km$^2$. Thus, the impact of the wind forcing alone can explain almost 50% of the prediction error for ice extent.

The low error values in the hindcast of September ice extent do not guarantee that pond fraction can be used for real forecasts of Arctic September sea ice, because for a forecast only data of previous years are available to calculate the weights and linear regression. Using only data from all previous years, we developed a forecast method based on the correlation between pond fraction and September ice extent (see last paragraph of Methods for details). The forecast skill $S$ is determined relative to a reference value:

$S = 1 - \sigma_{\text{ferr}^2}/\sigma_{\text{ref}^2}$, where $\sigma_{\text{ref}} = 0.57$ million km$^2$ is the square root of the variance of de-trended observed ice extent and $\sigma_{\text{ferr}^2}$ is the forecast error variance. Figure 4b,c shows that the error of our predicted September ice extent is larger for the forecast mode than for the hindcast. Nevertheless, our error value of $\sigma_{\text{ferr}} = 0.44$ million km$^2$ (forecast based on pond fraction from 1 May to 25 June) and our skill value of $S = 0.41$ are remarkable in comparison to negative skill values for statistical forecasts reported in the literature[5]. The corresponding anomaly correlation coefficient ACC $= 0.65$ is even higher than the value of 0.60 for seasonal September ice forecast with a global climate model-based prediction system that accounts for the atmospheric conditions between June and September[7]. Note that we are able to predict the observed September ice area with a similar degree of skill as the observed ice extent (Supplementary Fig. 2). The choice of the applied SSM/I algorithm (NASA Team or Bootstrap) does not materially affect our results (Supplementary Figs 2 and 3).

A forecast based on the amount of thin ice has a lower skill ($S = 0.29$, Fig. 4b) than that based on pond fraction ($S = 0.41$). However, the fact that there is any skill at all using thin ice confirms that our model simulation is realistic with the inclusion of the melt-pond model. The differences between simulated and observed sea-ice extent are small (Fig. 2 for 1996 and 2012). If we use the pond statistics based on MODIS satellite data[16], we get a similar correlation by integrating over the period May until July, but the period for which MODIS is available (since 2002) is too short to draw statistically valid conclusions.

The CICE simulation in this study uses NCEP_Reanalysis-2 data[13] for the atmospheric forcing which are available with a delay of less than one day. Therefore, we can carry out a CICE simulation to obtain the pond fraction and to forecast the September ice extent with an accuracy of 0.50 million km$^2$ by the beginning of June (May pond fraction) and with an accuracy of 0.44 million km$^2$ by the end of June. For September 2013 we forecast a mean ice extent of $5.55 \pm 0.44$ million km$^2$, which is closer to the observed mean value of 5.35 million km$^2$ than any of the 23 statistical, model and heuristic predictions presented at the Arctic Sea Ice Outlook webpage[21] in July (median value of 4.0 million km$^2$).

The World Climate Research Programme CMIP5 climate modelling study reveals that the spread of Arctic September sea ice between the individual members is considerable (for example, September 2000 ice extent varies between 2 and 12 million km$^2$)

355

and that the observed downward trend is still not fully captured[3]. Statistical predictions of ice extent cannot take into account the coupled interactions and feedbacks between sea ice and atmosphere[6–8]. For operational forecasts of seasonal sea ice, a coupled atmosphere–sea-ice–ocean model-based prediction system that accounts for these interactions seems to be best suited. Our calculations show that the increase of melt-ponds (4%/decade in July) results in the observed decrease in summer albedo (3%/decade in July/August; ref. 22). The results of this study demonstrate that the inclusion of our melt-pond model promises to improve the prediction of Arctic September ice extent substantially. We conclude that the inclusion of a realistic melt-pond model will transform future forecast and climate models in the Arctic regions and beyond.

## Methods

The Los Alamos sea-ice model CICE (refs 12,23) is a dynamic-thermodynamic sea-ice model designed for inclusion within a global climate model. We have implemented two new processes into CICE: a prognostic model for melt-ponds[10] and an elastic anisotropic-plastic (EAP) model that explicitly accounts for the observed sub-continuum anisotropy of the sea-ice cover[24,25]. The principal concept of our melt-pond model is that the melt water, formed as a result of snow melt, ice melt and precipitation, runs downhill under the influence of gravity and collects on sea ice starting at the lowest surface height[10,26,27]. Applying our melt-pond model and our EAP model, we performed a stand-alone sea-ice simulation for the pan-Arctic region (~40 km grid resolution) over the period 1979 to September 2013 using NCEP_Reanalysis-2 (ref. 13) data as atmospheric forcing. CICE contains a simple mixed-layer ocean model with a prognostic ocean temperature. To account for heat transport in the ocean, we restore the mixed-layer ocean temperature and salinity to climatological monthly means from MYO-WP4-PUM-GLOBAL-REANALYSIS-PHYS-001-004 (ref. 28) with a restoring timescale of 20 days. No ocean current is applied.

To investigate the impact of the wind forcing during summer on the September ice extent, we performed $35 \times 35$ three-month-long sensitivity studies, in which we replaced the wind forcing of the current year by the wind fields of all other years (1979–2013) for the period 26 June to 30 September.

For making real forecasts, we carried out 30 further CICE simulations from 1 June to 30 September for the years 1984–2013. We generate forcing data for this period by calculating five-year six-hourly, daily and monthly means from the previous five years of NCEP forcing and take into account the trend from 1979 to the year of forecast. The mean was calculated for all atmospheric forcing data apart from the wind vector. Because averaging the wind velocity vector would reduce the wind speed, we applied the wind forcing from 1983 (an average year with respect to ice advection) for all further simulations. The simulated September ice extent of these simulations is used only to calculate the spatial weights for pond and thin-ice fraction.

We calculated the Pearson product moment correlation coefficient $R$ for the de-trended time series of pond and thin ice fraction with the de-trended time series of September ice extent. The given $p$-values are based on an F test. To determine the time series we integrate pond and thin-ice fraction over time and space. We apply several temporal integration periods varying from 1 May to 16 May up to 1 May to 30 July. For the spatial integration, we first determine weights for each grid point following the method described in ref. 5. The weights are determined as the magnitude of $R$ of the de-trended time series of pond and thin-ice area for each grid point with the de-trended time series of total September ice extent. Most of the grid points have a negative $R$. For grid points with a positive $R$ the weight is set to zero. As an example, grid points with $R < -0.3$ (for pond fraction integrated from 1 May to 25 June) are marked by crosses in Fig. 2a.

We used a linear regression model to forecast September ice extent $f(y)$ using the pond or thin-ice fraction as the predictor $x(y)$. The regression equation is: $f(y) = a + bx(y) + \varepsilon(y)$, with $y$ indicating the years from 1979 to 2013, $\varepsilon$ the error, with the constants $a$ and $b$ determined by a least squares procedure. For verification, we distinguish between a hindcast and a forecast. For the hindcast, we apply data from all years to calculate the weights, the linear regression and the prediction error variance $\sigma_{perr^2}$. The weights are determined as the magnitude of the local correlation coefficient $R$ between the de-trended time series of pond (and thin-ice) fraction with the de-trended time series of total September ice extent. For the forecast, we use data only from previous years. To utilize the pond (and thin-ice) information of the current spring for the September ice forecast, we include for the calculation of weights the September ice extent from our CICE simulation of the current year with atmospheric forcing from previous years. Afterwards, data only from previous years are applied to calculate the linear regression and the error of the forecast year (for 1984–2013). The forecast skill is

$S = 1 - \sigma_{ferr^2}/\sigma_{ref^2}$, where $\sigma_{ref^2}$ is the variance of the de-trended climatology and $\sigma_{ferr^2}$ the forecast error variance.

## References

1. Cavalieri, D., Parkinson, C., Gloersen, P. & Zwally, H. J. *Sea Ice Concentrations from Nimbus-7 SMMR and DMSP SSM/I-SSMIS Passive Microwave Data.* [1979–2012]. (NASA DAAC at the National Snow and Ice Data Center, 1996, updated 2013).
2. Perovich, D. K. & Richter-Menge, J. A. Loss of sea ice in the Arctic. *Ann. Rev. Mar. Sci.* **1**, 417–441 (2009).
3. Stroeve, J. C. *et al.* Trends in Arctic sea ice extent from CMIP5, CMIP3 and observations. *Geophys. Res. Lett.* **39**, L16502 (2012).
4. Eicken, H. Arctic sea ice needs better forecasts. *Nature* **497**, 431–433 (2013).
5. Lindsay, R. W., Zhang, J., Schweiger, A. J. & Steele, M. A. Seasonal predictions of ice extent in the Arctic Ocean. *J. Geophys. Res.* **113**, C02023 (2008).
6. Sigmond, M., Fyfe, J. C., Flato, G. M., Kharin, V. V. & Merryfield, W. J. Seasonal forecast skill of Arctic sea ice area in a dynamical forecast system. *Geophys. Res. Lett.* **40**, 529–534 (2013).
7. Chevallier, M., Melia, D. S. Y., Voldoire, A., Deque, M. & Garric, G. Seasonal forecasts of the pan-Arctic sea ice extent using a GCM-based seasonal prediction system. *J. Clim.* **26**, 6092–6104 (2013).
8. Wang, W., Chen, M. & Kumar, A. Seasonal prediction of Arctic sea ice extent from a coupled dynamical forecast system. *Mon. Weat. Rev.* **141**, 1375–1394 (2013).
9. Blanchard-Wrigglesworth, E., Armour, K. C., Bitz, C. M. & DeWeaver, E. Persistence and inherent predictability of Arctic sea ice in a GCM ensemble and observations. *J. Clim.* **24**, 231–250 (2011).
10. Flocco, D., Schröder, D., Feltham, D. L. & Hunke, E. C. Impact of melt ponds on Arctic sea ice simulations from 1990 to 2007. *J. Geophys. Res.* **117**, C09032 (2012).
11. Perovich, D. K. *et al.* Transpolar observations of the morphological properties of Arctic sea ice-albedo. *J. Geophys. Res.* **114**, C00A04 (2009).
12. Hunke, E. C., Lipscomb, W. H., Turner, A. K., Jeffrey, N. & Elliot, S. CICE: The Los Alamos Sea Ice Model, Documentation and Software User's Manual, Version 5.0. Tech. Rep. LA-CC-06-012, Los Alamos National Laboratory. Available at: http://climate.lanl.gov/Models/CICE (2013).
13. Kanamitsu, M. *et al.* NCEP-DOE AMIP-II Reanalysis (R-2). *Bull. Am. Meteorol. Soc.* **1631–1643** (2002, updated 2013).
14. Fetterer, F. & Untersteiner, N. Observations of melt ponds on Arctic sea ice. *J. Geophys. Res.* **103**, 24821–24835 (1998).
15. Eicken, H., Grenfell, T. C., Perovich, D. K., Richter-Menge, J. A. & Frey, K. Hydraulic controls of summer Arctic pack ice albedo. *J. Geophys. Res.* **109**, C08007 (2004).
16. Rösel, A. & Kaleschke, L. Exceptional melt pond occurrence in the years 2007 and 2011 on the Arctic sea ice revealed from MODIS satellite data. *J. Geophys. Res.* **117**, C05018 (2012).
17. Perovich, D. K., Nghiem, S. V., Markus, T. & Schweiger, A. Seasonal evolution and interannual variability of the local solar energy absorbed by the Arctic sea ice–ocean system. *J. Geophys. Res.* **112**, C03005 (2007).
18. Maslanik, J., Drobot, S., Fowler, C., Emery, W. & Barry, R. On the Arctic climate paradox and the continuing role of atmospheric circulation in affecting sea ice conditions. *Geophys. Res. Lett.* **34**, L03711 (2007).
19. Parkinson, C. L. & Comiso, J. C. On the 2012 record low Arctic sea ice cover: Combined impact of preconditioning and an August storm. *Geophys. Res. Lett* **40**, 1356–1361 (2013).
20. Scott, F. & Feltham, D. L. A model of the three-dimensional evolution of Arctic melt ponds on first-year and multiyear sea ice. *J. Geophys. Res.* **115**, C12064 (2010).
21. Overland, J., Eicken, H. & Tivy, A. http://www.arcus.org/search/seaiceoutlook/2013/june (2013).
22. Riihelä, A., Manninen, T. & Laine, V. Observed changes in the albedo of the Arctic sea-ice zone for the period 1982–2009. *Nature Clim. Change* **3**, 895–898 (2013).
23. Hunke, E. C. & Dukowicz, J. K. An elastic viscous plastic model for sea ice dynamics. *J. Phys. Oceanogr.* **27**, 1849–1868 (1997).
24. Tsamados, M., Feltham, D. L. & Wilchinsky, A. V. Impact of a new anisotropic rheology on simulations of Arctic sea ice. *J. Geophys. Res.* **118**, 91–107 (2013).
25. Wilchinsky, A. & Feltham, D. Modelling the rheology of sea ice as a collection of diamond-shaped floes. *J. Non-Newtonian Fluid Mech.* **138**, 22–32 (2006).
26. Flocco, D. & Feltham, D. L. A continuum model of melt pond evolution on Arctic sea ice. *J. Geophys. Res.* **112**, C08016 (2007).

27. Flocco, D., Feltham, D. L. & Turner, A. K. Incorporation of a physically based melt pond scheme into the sea ice component of a climate model. *J. Geophys. Res.* **115,** C08012 (2010).
28. Ferry, N. *et al.* Product User Manual GLOBAL-REANALYSIS-PHYS-001-004-a and b (MyOcean, Eur. Comm., Brussels (2011).

## Author contributions
D.F., D.L.F and D.S. developed the melt-pond model. M.T. and D.L.F. developed the EAP model. D.S. performed the CICE simulations and the statistical calculations. All authors discussed the results.

## Additional information
Supplementary information is available in the online version of the paper. Reprints and permissions information is available online at www.nature.com/reprints. Correspondence and requests for materials should be addressed to D.S.

## Competing financial interests
The authors declare no competing financial interests.